ELSEVIER

International Journal of Mass Spectrometry 223–224 (2003) 783–801

International Journal of Mass Spectrometry

www.elsevier.com/locate/ijms

Dynamics of hyperthermal energy ion–surface collisions: dissociative and non-dissociative scattering of ethanol cations from a self-assembled monolayer surface of fluorinated alkyl thiol on Au (1 1 1)

Anil K. Shukla*, Jean H. Futrell

William R. Wiley Environmental Molecular Sciences Laboratory, Pacific Northwest National Laboratory, P.O. Box 999, Richland, WA 99352, USA

Received 15 August 2002; accepted 3 September 2002

Abstract

Dissociation and inelastic scattering of ethanol molecular ions from self-assembled monolayer (SAM) surface of fluorinated alkyl thiol on an Au (1 1 1) monocrystal have been studied at 28.9 and 52.9 eV collision energies. A single dynamics mechanism for quasi-inelastic scattering was found at both energies. Ions recoil nearly parallel to the surface with very small kinetic energy losses of the order of $\leq$2 eV. Dissociation dynamics features for the main dissociation channel, loss of methyl radical, are dramatically different from that of inelastically scattered primary ions and are different at the two collision energies studied. At 28.9 eV two energetically and angularly resolved features are observed, one corresponding to the loss of very large amounts (nearly all) of ion's translational energy and the other appearing to gain energy (superelastic scattering). This dynamics feature is interpreted as delayed dissociation of ions transmitted through the energy analyzer as molecular ions. This implies a lifetime of such excited ions of more than 5 μs. The same dynamics features are observed at 52.9 eV ion energy except that a second inelastic process begins to compete with the nearly fully inelastic process. Moreover, at this energy the delayed ion dissociation mechanism is the dominant mechanism. The hypothesis that collision of ethanol cations with the SAM surface initially involves collision of the ion with a single end group of the SAM polymer chain provides a useful rationale for the observed dynamics. Support for this hypothesis is provided by Newton diagrams, which summarize momentum conservation relationships in terms of a common center-of-mass, CM_{eff}, which provides a basis for describing scattering mechanisms for this system. Observation of three energetically distinct scattering processes suggests uniquely different ion–surface interactions contributing to surface-induced dissociation of ethanol ions. Preliminary experiments with Ar^+ scattered from the same surface exhibit very similar dynamics features to that observed for ethanol cations. Finally, we note that intensities of scattered primary or fragment ions never approach the specular angle at the energies investigated here. (Int J Mass Spectrom 223–224 (2003) 783–801)

Keywords: Ion–surface collisions; Surface-induced dissociation; Self-assembled monolayer surface; Inelastic collisions; Energy transfer; Scattering; Ethanol ions

* Corresponding author. E-mail: anil.shukla@pnl.gov

1387-3806/02/$ – see front matter
PII S1387-3806(02)00982-X

1. Introduction

Ion–surface interactions are important in many aspects of science and technology, such as catalysis, microelectronics and surface characterization [1,2]. Low energy ion scattering has been extensively used for determining both surface composition and crystallographic structure [3,4]. Most studies carried out with these motivations have involved monatomic or diatomic ions and have covered a wide range of ion kinetic energies. Recently, ion–surface collisions have been extended to include polyatomic ions and clusters with emphasis on their internal excitation and subsequent dissociation [5]. For polyatomic ions the latter class of experiments is a growing segment of analytical mass spectrometry and is described as surface-induced dissociation (SID). It is in many ways analogous to gas phase collision-induced dissociation (CID) in tandem mass spectrometry. Coinciding with the ability of mass spectroscopists to ionize biological molecules and polymers, ion–surface collisions are increasingly used for the characterization of peptides and proteins and other complex molecules [6–11]. It can be argued that SID is an especially important technique for fragmenting and characterizing biological molecules and polymers, principal current goals of analytical mass spectrometry.

The basic phenomena of ion activation and dissociation in SID, by analogy to CID involve collisional activation of ions, which then decompose unimolecularly [12,13]. It must be kept in mind, however, that ion collisions with a clean metal surface of low work function result almost entirely in the neutralization of the colliding ions, with only a small fraction (<0.1%) scattered off the surface and detected as fragment ions [14]. To enhance the yield of useful SID ions modified surfaces—especially self-assembled monolayers (SAMs) of alkyl thiols and fluorinated alkyl thiols—on gold has been used [15–17]. With SAM surfaces, ions are blocked from interacting directly with the metal substrate by tightly packed monolayer molecules [18], thus reducing ion neutralization.

Although several research groups are using SID for ion characterization, there have been relatively few studies of the mechanism(s) and the extent of energy transfer and subsequent dissociation of polyatomic ions in ion–surface collisions. Early studies have used fragment ion intensities of "thermometer ions" or fragment spectra of model compounds modeled by a combination of experimental breakdown graphs (or those calculated from statistical theories) with parameterized energy transfer distributions [19–22]. Recent combined experimental and modeling studies have concluded that ions do not collide with the bulk surface or the whole SAM molecule but rather the end group or a small chain length at the end of it [10,20]. Similar conclusions were reached in recent experimental studies [14,23] of the SID of benzene and carbon disulfide ions with a SAM surface using a modified crossed-beam instrument. These studies measured fragment ion intensities and their energy distributions as a function of the scattering angle. Among interesting results obtained from these molecular beam studies in our laboratory and analogous studies by Herman and coworkers was determination that scattering of the fragment ions is non-specular and that the energy lost by the projectile ions in both dissociative and non-dissociative scattering was very large, often approaching the total ion kinetic energy [14,22,23–26]. Clearly a very large fraction of the ion's kinetic energy is transferred into surface modes and only a small fraction is converted from kinetic energy into internal modes of the projectile ions.

The extent and mechanism of dissociation in a collision process depends strongly on the efficiency of energy transfer. From the velocity distributions (converted from energy distributions using the relationship $E = \frac{1}{2}mv^2$) of the fragment ions and undissociated primary ions, it was concluded for both benzene and ethanol molecular ions that ions dissociate unimolecularly after leaving the surface [14,24–26]. However, when the dissociation time-scale is much shorter than the calculated lifetime from statistical theories of unimolecular decay, this mechanism is no longer tenable. A transition from statistical to non-statistical decay inevitably takes place as the lifetime is decreased. One such mechanism for non-statistical dissociation

proposed by Hanley and coworkers [27] for dissociation of $Si(Me)_3^+$ and by Levine and coworkers for cluster ions [28,29] is the shattering mechanism.

The shattering mechanism and a transition from post-surface to on-surface dissociation mechanisms is supported by a series of trajectory simulations of energy transfer and dissociation dynamics carried out by Hase and coworkers [30,31]. They also found that the nature of the surface is an important variable where they modeled collisions of several different ions, including small peptides with SAM (*n*-hexyl thiol) and diamond surfaces. Using an analytic potential energy function for $Cr(CO)_6^+$ ions interacting with the two types of surfaces, they found very different collision dynamics for "soft" SAM and "hard" diamond surfaces. Dissociation from a SAM surface follows the statistical theories of unimolecular dissociation while collisions with a diamond surface results in the shattering of the ion. Energy transfer into internal modes from collision with diamond surface is considerably higher than for the SAM surface. This is also predicted for other ions, such as small peptides. For example, combination of shattering and delayed dissociation is predicted for protonated glycine impacting on an alkyl thiol surface [32].

We have recently constructed an ion beam scattering instrument for investigating dynamics of the SID processes by measuring the energy and intensity distributions of scattered primary and fragment ions as a function of scattering angle [33]. Our intent is to utilize this apparatus to investigate several of the dynamics features of SID outlined above. In this paper we present our first results on SID dynamics for the ethanol molecular ion at two collision energies, 28.9 and 52.9 eV. The ethanol ion was chosen because it has been studied extensively by Herman and coworkers using a variety of surfaces to which our results may be compared. Our results for colliding ethanol ions with a SAM surface of fluorinated alkyl thiol on gold monocrystal (1 1 1) are quite consistent with prior work by Herman and coworkers [22,25,26]. In addition some entirely new features in the energy and angular distributions of scattered primary and fragment ions have been discovered.

2. Experimental

Fig. 1 shows a schematic of the instrument used for our SID experiments. The instrument has been described in detail elsewhere [33] and only salient features are given here. Primary ethanol molecular ions are formed by 70 eV energy electrons and accelerated to ~1250 eV for mass and energy analysis using a double focusing reverse geometry mass spectrometer (JEOL—GCmate). The mass and energy selected ion beam is transferred into a collision chamber through a 2 mm aperture and decelerated to desired kinetic energy by a series of cylindrical tube lenses. The ion beam is collimated by a 2 mm aperture and collides with a surface at a fixed angle, which has been set to 45° with respect to the surface normal in the experiments reported here. Scattered primary and fragment ions are energy analyzed by a 160° spherical energy analyzer, mass analyzed by a quadrupole mass filter and detected by a channel electron multiplier operating in pulse counting mode. The energy analyzer, quadrupole mass filter and the detector are rotated with respect to the collision center to measure energy and intensity distributions of all ions as a function of scattering angle.

The collision region, surface, last lens element and the first entrance aperture to the energy analyzer are all maintained at the same potential to minimize field penetration effects which would interfere with their apparent angular scattering distributions. The energy analyzer and quadrupole mass filter are floated at higher potentials using the ion source voltage as reference to decrease ion kinetic energy and increase both energy and mass resolution of the second stage analyzer. The primary ion beam at ~50 eV energy has an angular distribution of ~2° (FWHM) and energy distribution of ~2.5 eV (FWHM). The energy resolution for the present experiments is set at $E/\Delta E = 50$ and the angular resolution at 3°. All angle measurements are made with respect to the surface normal as shown in the inset of Fig. 1.

The energy analyzer is operated in constant transmission mode and constant energy resolution mode to avoid any discrimination of low energy ions by the

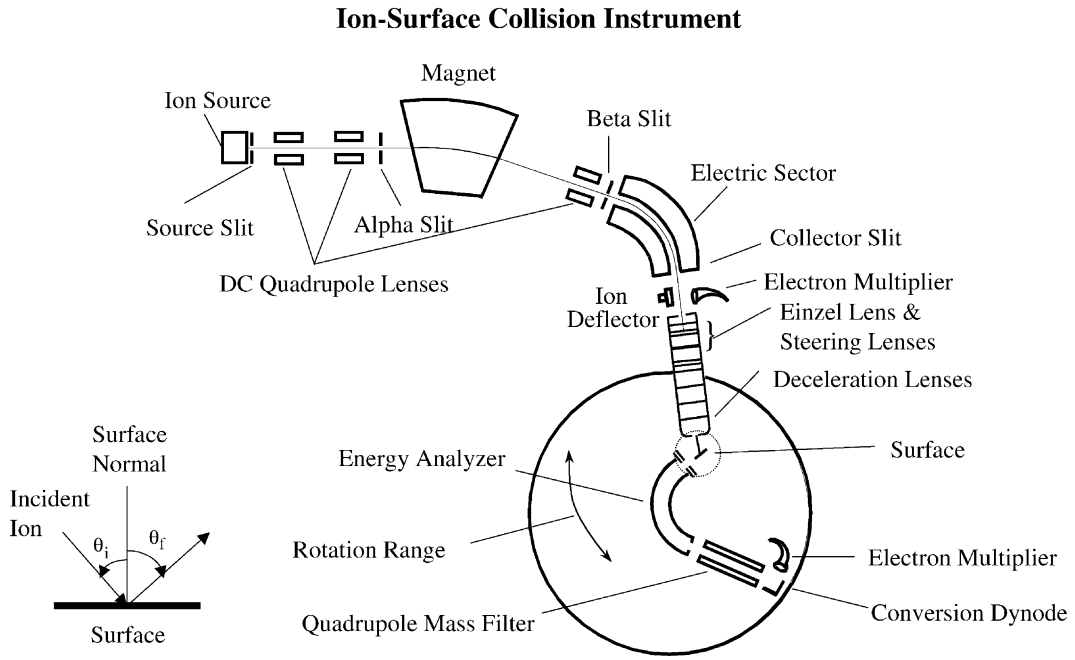

Fig. 1. Schematic of the beam scattering instrument. The inset gives the definition of the angle of incidence and scattering angles. See discussion in the text.

analyzer. This requires that all ions pass through the energy analyzer at the same ion energy, 100 eV for the present experiments. As primary ions dissociate, their kinetic energy is reduced by the mass ratio of the fragment and the parent ion (31:46 for ethanol ions). In order for these fragment ions to pass through the energy analyzer at fixed ion energy of 100 eV, these lower energy ions are accelerated by the energy difference between the primary ions and the fragment ions in addition to any energy lost in the collisional activation step. Scattered primary ions are similarly accelerated after surface collision to pass through the energy analyzer if they lose energy in collision. For this reason, all scattered ions are observed at higher ramp voltages than primary ions.

The SAM surface was prepared from the fluorinated alkyl thiol ($F_3C(CF_2)_9(CH_2)_2SH$) by immersing the gold crystal (Au, 1 1 1) in 1 mM ethanol solution of the SAM material for more than 24 h after cleaning in a UV cleaner and in ethanol using an ultrasonic cleaner. Excess SAM material was removed from the surface by sonicating the surface in ethanol for another 5 min before transferring it into the vacuum system. The vacuum chamber was pumped at least overnight before any SID experiments were performed so that remaining solvent is removed from the surface. The mass spectrometer and the collision chamber are all pumped by turbo molecular pumps and the background pressure in the collision chamber is $\sim 3 \times 10^{-7}$ Torr.

3. Results and discussion

The thermochemistry of the dissociation of ethanol molecular ion is well established [34]. Its ionization energy is 10.48 eV and appearance energies of main fragments are as follows: $C_2H_5O^+$ (10.7 eV), CH_2OH^+ (11.2 eV), $C_2H_5^+/CHO^+$ (12.7 eV) and $C_2H_3^+$ (14.7 eV). We observe all these fragment ions at both 28.9 and 52.9 eV. Since their energy distributions and dissociation dynamics are similar to the main fragmentation channel of CH_3 elimination we

will discuss in this paper only the dynamics for the formation of CH_2OH^+ ions and inelastically scattered parent ions.

3.1. Non-dissociative inelastic scattering of parent ions

Figs. 2 and 3 show the raw energy distributions of scattered ethanol ions as a function of scattering angle at 28.9 and 52.9 eV, respectively. In these figures, the raw data are shown for a series of angles which include all the observed intensity in a typical experiment. Curves are offset, as shown by slanted lines, to define the ion intensity as a function of ion kinetic energy. As discussed in Section 2, ramp voltages were transformed into ion kinetic energy by subtracting the center-line voltage from the ramp voltage. The corresponding angular distributions are shown as polar plots of summed intensity at each angle as a function of scattering angle in Figs. 4 and 5. Clearly the intensity distributions of scattered molecular ions are sharply peaked in both energy and angle. In particular, ion distributions at both collision energies are sharply peaked at about 85°, with respect to the surface normal

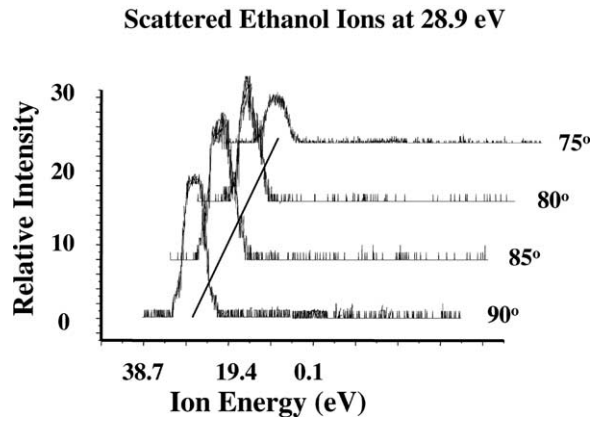

Fig. 2. Kinetic energy distributions of scattered ethanol ions at 28.9 eV collision energy, plotted as a function of scattering angle. Successive scans are offset as indicated. The solid line marks the primary ion kinetic energy.

and have half-widths of less than 5°. Since the energy width of the primary ion beam is ∼2.5 eV FWHM and the resolution of the scanning energy analyzer is 2 eV, the minimum peak width is ∼6 eV. Since the observed peak width is of this order we infer that the intrinsic width of the scattered primary ion is <2 eV.

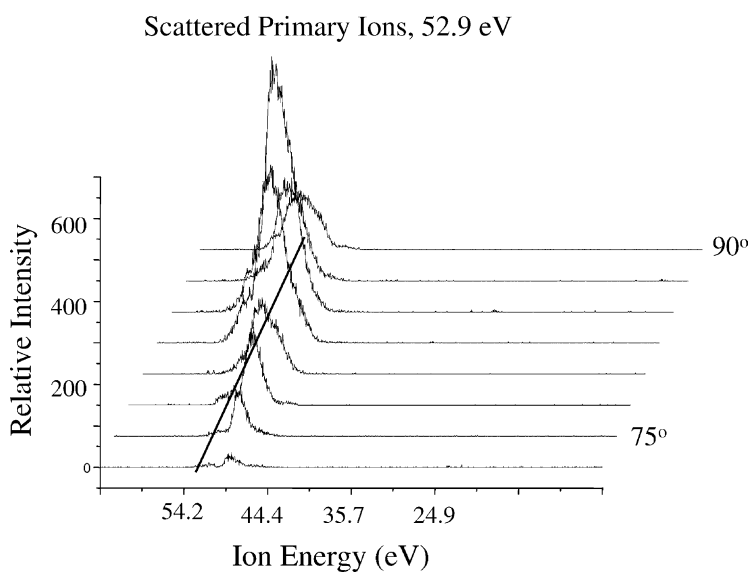

Fig. 3. Kinetic energy distribution of scattered ethanol ions at 52.9 eV collision energy at the indicated scattering angles. Successive scans are offset as indicated. Solid line marks the kinetic energy of the primary ion beam.

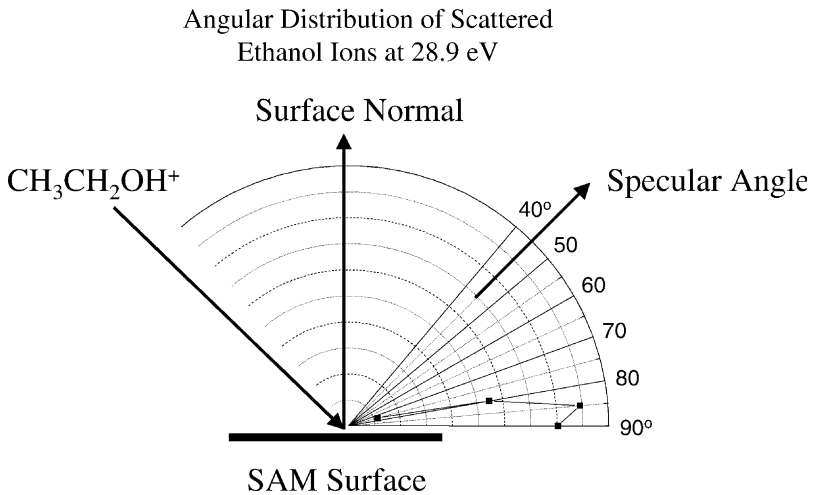

Fig. 4. Angular distribution of scattered ethanol ions at 28.9 eV. Intensities are summed at each angle and plotted as a function of angle.

Considering both the energy (2 eV) and angular (3°) resolutions of our detector, the remarkably sharp distribution found experimentally shows that recoiling ions are scattered only a few degrees from parallel to the SAM surface with very modest loss in kinetic energy.

Kinetic energy lost by scattered ethanol ions after colliding with the SAM surface is given in Figs. 6 and 7 for 28.9 and 52.9 eV ion energies, respectively. At both energies there is a trend of increased energy loss as scattering angle decreases, moving away from the surface toward the specular angle. Evidently conversion of translational energy into internal energy—as measured with energy loss by impacting ions—increases with decreasing scattering angle. Therefore, ions scattered along the surface parallel may be described as relatively "soft" collisions while those scattered at larger angles are from relatively "hard" collisions. As noted previously, the energy

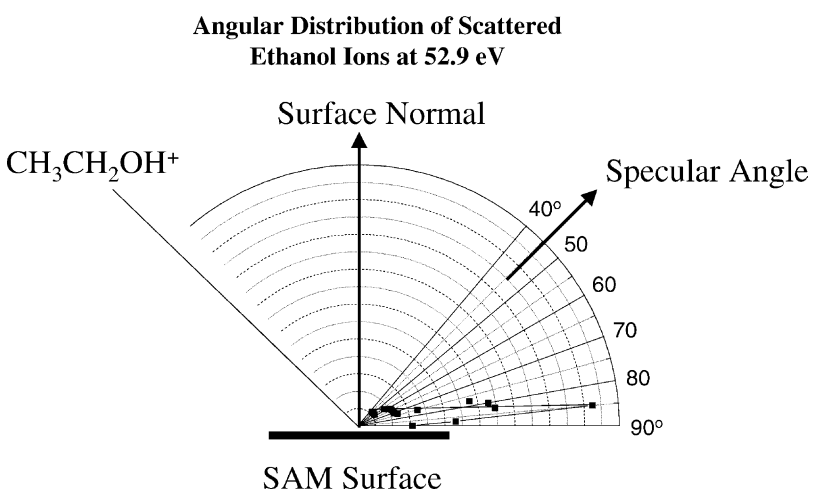

Fig. 5. Angular distribution of scattered ethanol ions at 52.9 eV.

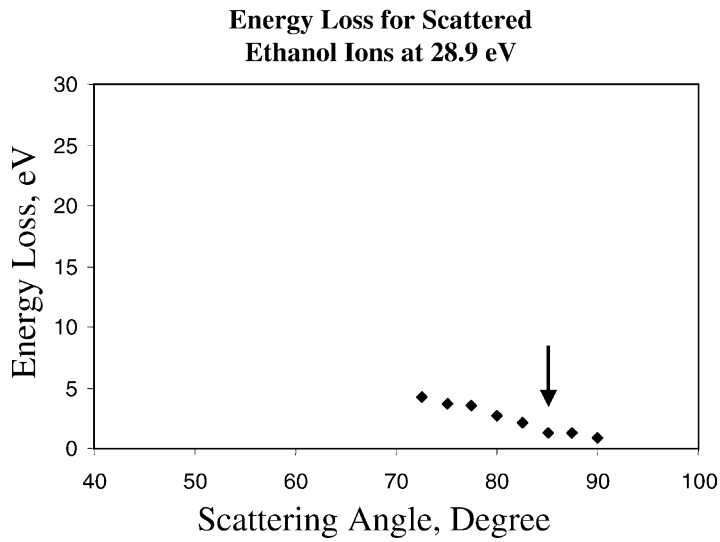

Fig. 6. Kinetic energy lost by scattered acetone ions at 28.9 eV plotted as a function of scattering angle. Arrow designates the most probable scattering angle.

width at both energies is quite narrow; the most probable energy is designated by vertical arrows in both figures. The maximum energy lost by scattered ethanol ions at the most probable scattering angle at both energies is nearly the same, $\sim 2.0 \pm 0.5$ eV. Since the maximum energy that can be transferred into ethanol ions without fragmenting them is 0.2 eV, most of the kinetic energy lost for even the weakly inelastic scattering mechanism is dissipated into the SAM surface.

It is interesting that kinetic energy losses for the inelastic scattering of benzene and carbon disulfide ions studied earlier at similar ion energies were much larger; approaching the total ion collision energy [14,23]. The difference is partially explained by the dissociation thermochemistry of these ions. Both

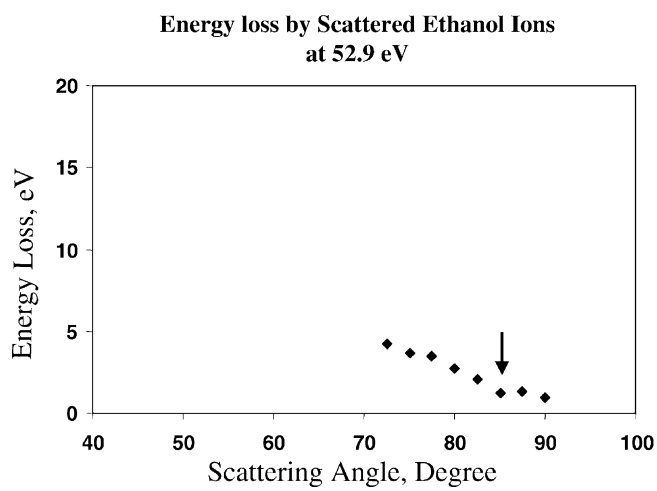

Fig. 7. Kinetic energy lost by scattered acetone ions at 52.9 eV plotted as a function of scattering angle. Arrow designates the most probable scattering angle.

benzene and carbon disulfide ions require ∼4.8 eV internal energy to promote their dissociations while the lowest energy channel in ethanol ion (loss of a hydrogen atom) is only 0.2 eV. Thus, ethanol ions begin to fragment at much lower internal excitation compared to benzene and carbon disulfide ions. It is very likely that the limited stability of the ethanol cation is a key restriction on the specific dynamics of inelastic scattering. However, both the angular scattering dynamics of carbon disulfide cations and ion energetics are quite different from ethanol cations and the limited stability of ethanol cation is only part of the story.

As noted earlier polar plots by the Herman group show a similar distribution for quasi-elastically scattered ethanol cations impacted on carbon and metal surfaces coated with chemisorbed hydrocarbon layers. The sharp peaking nearly parallel to the surface in both their work and ours suggests a "skipping" dynamics model. This feature plus the low energy loss strongly implies the effective surface potential seen by the scattered ethanol ions is nearly flat. We suggest that this shape of the potential seen by the ion, plus the low threshold for its dissociation, are important factors. We also note that the observed dynamics are for surviving ethanol cations, not the total distribution of internally excited cations following SAM collisional excitation.

Rather similar angular distributions have been reported for scattering of surviving ions from clean metal surfaces [35]. The mechanism suggested is surface trapping, resulting from a neutralization and re-ionization mechanism, which traps some low energy ions within the surface and releases others—the surviving ions—after multiple collisions. The skipping motion is the result of ion interactions with the effective potential generated as the ion approaches the surface. For clean metal surfaces the total potential seen by the ion is obtained by combining the image charge with a repulsive potential (for non-reactive ions). For low energy ions (<100 eV) and large incidence angle the surface potential appears nearly flat. When a substantial amount of ion kinetic energy is dissipated in phonon and plasmon interactions, velocity components are mixed and a narrow cone of scattered ion intensity nearly parallel to the surface results.

Although this mechanism cannot apply to scattering from SAM surfaces it suggests some analogies which may be applicable. Results presented later in this paper further support the concept that the initial scattering event involves interaction with the end group of the SAM molecular chain. Accordingly, collision theory concepts which describe gas phase collisions [36,37] assuming a two-body effective potential is a useful first-order description of the initial interaction. After the initial interaction ions scattered along the surface with large impact parameters experience a nearly flat potential analogous to that described for ions interacting with metal surfaces. A very important difference from ion–metal interactions is that SAMs shield the ions from the Fermi level and image charge potential. Accordingly, the number of surviving ions is much greater than for metals but still only a few percent of the impacting ion beam.

3.2. Dissociative scattering

Figs. 8 and 9 are plots of measured energy distributions of scattered CH_2OH^+ fragment ions at 28.9 and 52.9 eV ion energy, respectively. Analogous to Figs. 2 and 3, these plots show typical experimental results for ion intensity as a function of ion kinetic energy at several angles. At 28.9 eV, there are two energetically distinct peaks, one corresponding to high kinetic energy loss that is much broader in energy and angle and a high kinetic energy peak which is observed in only a narrow angle range near the surface parallel. The broad peak at low kinetic energy (high energy loss) is in good agreement with earlier investigation of the SID of ethanol ions in the energy range of 22–32 eV by Herman and coworkers [23–26]. These investigators did not report the lower intensity narrow peak near the surface parallel observed in the present experiments.

As expected, dissociation channels are greatly enhanced in the results shown in Fig. 9a and b for 52.9 eV collision energy. There are now three peaks in these spectra that are distinguishable in their angular and energetic characteristics. Fig. 9b plots at higher amplification for clarity the highly endoergic, low kinetic

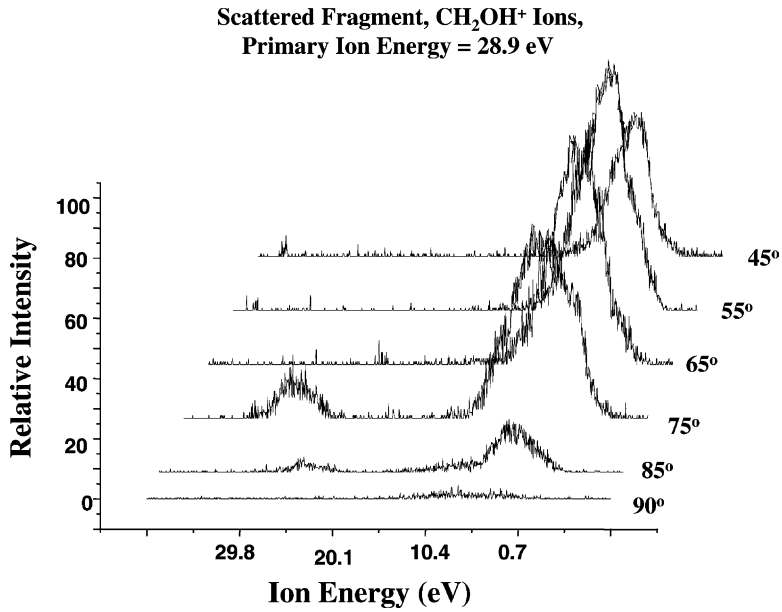

Fig. 8. Kinetic energy distributions of scattered fragment ions, CH_2OH^+, at several scattering angles from collisions of 28.9 eV energy ions with the SAM surface. Two mechanisms are shown as prompt and delayed dissociation, respectively. See discussion in the text.

energy fragment ion spectra. Two peaks are readily identified with those found at 28.9 eV collision energy and an additional peak at intermediate kinetic energy is detected at the higher collision energy.

Figs. 10 and 11 are polar plots showing the integrated ion intensity at each angle for CH_2OH^+ ions at 28.9 and 52.9 eV collision energies, respectively. Although the energy distributions overlap in both figures, the maximum of each energy distribution is located at a distinctive scattering angle. This enables a separation in scattering angle of three scattering mechanisms at 52.9 eV collision energy. Surprisingly, the high kinetic energy peak is of highest intensity and is sharply peaked at 85°, close to the surface parallel. Since the peaks scattered close to the surface parallel track the scattering cone of inelastically scattered primary ion beams at both energies, we infer that the same dynamical scattering process is involved.

Two energy loss processes, prompt and delayed dissociation, are depicted in Fig. 12. The prompt dissociation process assumes explicitly that ions dissociate immediately after recoiling from the surface (more explicitly, after recoiling from the surface as parent ions and prior to entering the energy analyzer). Accordingly, the measured kinetic energy is converted to the equivalent kinetic energy of its precursor parent ion in Fig. 12 by multiplying the measured energy by the ratio of parent to fragment ion masses as described in Section 2. The main fragment peak corresponds to very large energy loss, approaching the full-translational energy even though only a very small amount of energy (∼0.7 eV) is needed for this dissociation to take place. In agreement with previous measurements of kinetic energy of recoiling ions in SID by our laboratory and by Herman and coworkers [24–26] these observations demonstrate that only a small fraction of the total energy lost by the ion with surface collision is transferred into internal modes of the ions or retained as kinetic energy of recoiling ions. Clearly the main energy sink in SID is energy deposition into the surface. Fig. 12 also shows that kinetic energy loss increases slowly in going from the surface parallel towards the specular angle, just as is observed for the undissociated parent ions.

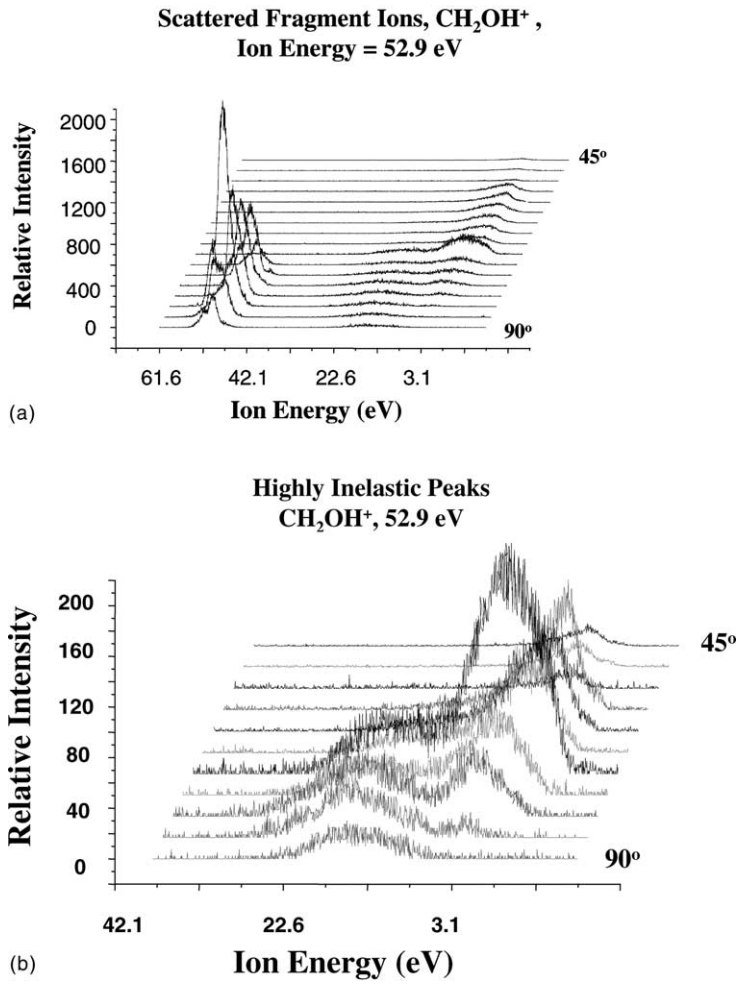

Fig. 9. (a) Kinetic energy distributions of scattered fragment ions, CH_2OH^+, at several scattering angles from collisions of 52.9 eV energy ions with the SAM surface. Two distributions labeled as prompt dissociation and one labeled as delayed dissociation, respectively, are shown. See discussion in the text. (b) Plot of the two smaller intensity peaks in the energy distributions of (a), enhanced for clarity.

The lowest energy loss peak in the energy spectra of the fragment ions from SID of 28.9 and 52.9 eV ethanol ions, observed close to the surface parallel, is markedly different energetically from the highly inelastic peaks described above. Correcting the measured fragment ion energy for the highest energy peak in Fig. 8 by the ratio of parent to daughter ion masses for prompt dissociation—we calculate an energy gain in SID of nearly 9 eV, which is an unacceptable result. An alternative interpretation is that these ions are formed by decomposition in the mass analyzer of ethanol cations that are transmitted by the energy analyzer as parent ions of *m*/*z* 46. This results in a very small endoergicity in the dissociation process—i.e., a normal inelastic scattering followed by decomposition. Accordingly, the data are plotted as delayed dissociation peaks in Figs. 12 and 13.

Kinetic energy lost by the ethanol ions for all three processes in SID at 52.9 eV is shown in Fig. 13. The two broad peaks correspond to very large kinetic energy losses, the nearly fully inelastic mechanism detected at 28.9 eV and discussed above, plus a

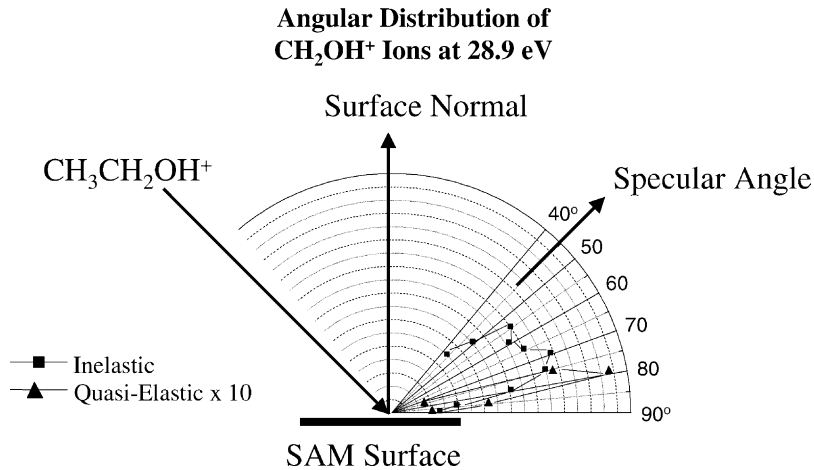

Fig. 10. Angular distributions of CH_2OH^+ fragment ions from quasi-elastic and highly inelastic dissociation processes at 28.9 eV collision energy. Intensities are summed at each angle and plotted as a function of angle.

second highly inelastic mechanism associated with energy losses varying between ∼25 and ∼30 eV. The highly inelastic mechanism was reported by Herman and coworkers, as noted earlier [24–26]. As ion energy is increased from 28.9 to 52.9 eV, a second and less inelastic process becomes competitive with the other two processes. The lowest energy loss peak from 52.9 eV collisions represents delayed dissociation of the parent ion and follows quite closely in angle and kinetic energy the inelastic scattering peak of primary ions. Interestingly, this peak has significantly increased in intensity at 52.9 eV approaching the intensity of the two inelastic peaks combined.

There are two possible mechanisms that may be suggested for the highly inelastic mechanism that generates product ions which recoil with low velocity

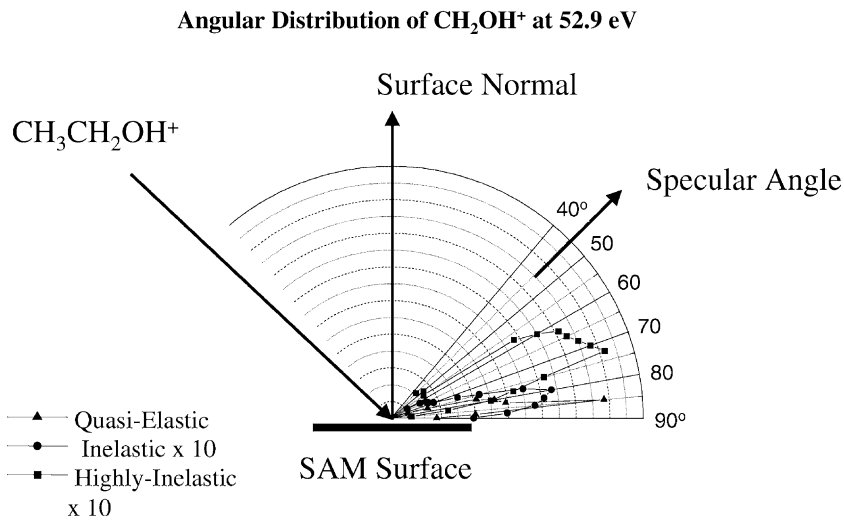

Fig. 11. Angular distributions of CH_2OH^+ fragment ions from collision of ethanol cations with the SAM surface at 52.9 eV collision energy. Intensities are summed at each angle and plotted as a function of angle.

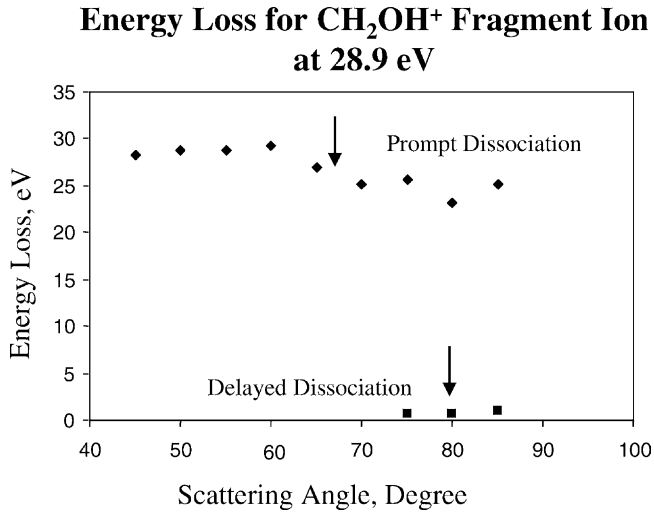

Fig. 12. Kinetic energy lost by dissociating primary ions in collision with the SAM surface at 28.9 eV ion energy. The prompt dissociation is highly inelastic, losing almost all ion kinetic energy. The delayed dissociation mechanism exhibits very modest loss of kinetic energy. See discussion in the text.

from the surface. One is the "shattering" mechanism described in Section 1. The other is a hard collision with a soft surface that transfers nearly all of its kinetic energy into the SAM surface, recoils with relatively low kinetic and internal energy and dissociates in the gas phase. Velocity analysis of ions scattered from hydrocarbon coated stainless steel, carbon and SAM surfaces in Herman's study of ethanol cation SID [24–26] in the same energy range support this mechanism. Since the angular scattering dynamics of the two studies are in very good agreement we favor this interpretation. However, the quite different scatter-

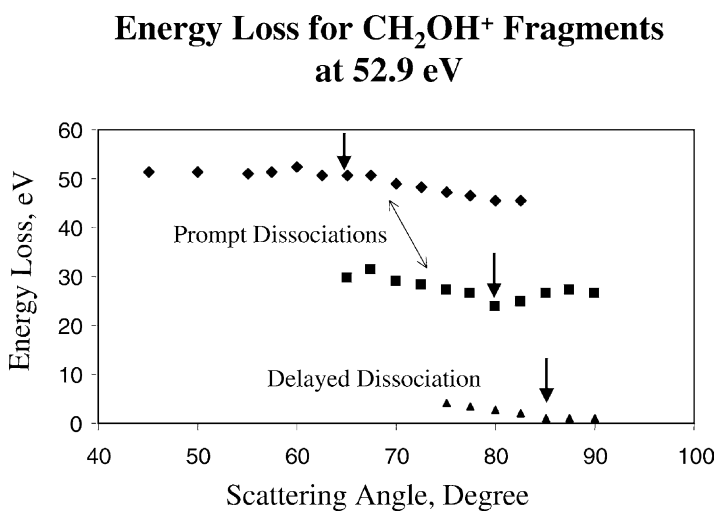

Fig. 13. Kinetic energy lost by dissociating primary ions in collision with the SAM surface at 52.9 eV ion energy. Three mechanisms are present. In addition to the two mechanisms in Fig. 12 there is an intermediate kinetic energy loss mechanism at this energy.

ing dynamics of surviving parent ions and fragment ions imply that different mechanisms are in play in our experiments with highly structured SAM surfaces prepared using a gold 1 1 1 crystal as the substrate.

The second mechanism shown in Fig. 12 corresponds in both scattering angle and energy to the weakly inelastically scattered primary ions, which are scattered nearly parallel to the surface. This interpretation is strongly supported by the 52.9 eV results in which this is the dominant mechanism. This delayed dissociation mechanism corresponds to quite long lifetimes for such a small cation. We calculate the time required to pass through both the collision region and the energy analyzer to be 5.4 and 4.0 μs at 26.9 and 52.9 eV, respectively. Survival of internally excited ethanol cations for such long times is quite remarkable. An RRKM [38] calculation of the rate for this dissociation process shows that this is a very fast dissociation, with a rate $\sim 10^8\,s^{-1}$ at threshold and no ions described by the simplest form RRKM model can possibly survive.

However, simple aliphatic alcohols, including ethanol, are in the class of exceptional small molecular ions known to have rates of unimolecular decay orders of magnitude lower than predicted by RRKM theory. There are a number of reasons that have been advanced to rationalize these results. These include the existence of low-lying isomers—distonic ions and ion–dipole complexes—and barriers, which may involve tunneling [36]. σ-Type ionization rather than n-type ionization may also extend lifetimes by introducing deeper potential wells than are otherwise anticipated. Extreme anharmonicity in these lengthened bond complexes may reduce unimolecular decay rates by orders of magnitude at internal energies near dissociation thresholds.

Theoretical calculations by Radom and coworkers [39] and Bouchoux and Choret [40] are informative but do not include sufficient information to support the dissociation dynamics needed for the present discussion. Early experimental data by Cooks et al. [41] reported formation of *m*/*z* 31, a metastable ion but later experiments by Stace and Shukla [42] concluded the apparent metastable ion was a CID product from background gases. This has been confirmed using a multi-sector mass spectrometer in our laboratory. In summary, we find no information from theory or from studies of gas phase dissociation of ethanol cations which helps us to rationalize our experimental results.

We turn therefore to the unusual dynamics of this SID channel and the close match of the delayed dissociation mechanism to the non-dissociative slightly inelastic scattering channel. We have suggested a skipping mechanism for these unusual dynamics in Section 3.1, in which ions initially scattered by a two-body collision, then interact with a nearly flat surface. Since the dynamics of this dissociation mechanism is identical in both angle and velocity to the non-dissociative channel, the conclusion they are linked is inescapable. Evidently, dissociation occurs for a population of parent ions which are scattered with multiple encounters from a flat potential surface and the perturbation causes them to dissociate at significantly lower rates than first-order RRKM rates and those observed mass spectrometrically.

Further evidence that the first step in this unusual dynamics feature is scattering from an effective mass rather than from a SAM chain or some collective interaction with a soft surface is given in the next section. The concept of a skipping mechanism referenced to a nearly flat surface has already been elaborated for weakly inelastic non-dissociative scattering of ethanol cations. Although it is incorrect to characterize this skipping mechanism as involving multiple interactions of trapped particles with the surface, the scattering of ions essentially parallel to the surface provides a mechanism for mixing of different states of the ion and exploring regions of their potential hypersurface which is not accessible to isolated gas phase ions. We suggest this as a hypothesis to rationalize extending ion lifetimes by orders of magnitude.

3.3. Newton diagrams and energy transfer

In this section we consider the construction of velocity plots for conservation of momentum for SAM surface collisions analogous to Newton diagrams for

gas phase collisions. In a gas phase crossed-beam experiment in which the neutral collider is atomic describing unique scattering events, the most probable velocities of fragment ions would be found on circles that have their origins on the relative velocity vector of the Newton diagram describing the collision process. Such a construction is impossible for surface scattering, since the surface blocks most of scattered products and since the surface is not a single particle obeying momentum conservation constraints. Despite these obvious differences, and for the reasons given earlier we analyze our SID data using the concept of an effective mass particle, which scatters incoming ions as the first step in the energy transfer mechanism. Since the "neutral particle" in our Newton diagram is at rest on the surface, the post-collision velocity of the primary ion beam can be identified with the relative velocity vector of conventional Newton diagrams [43]. We also show in Figs. 14 and 15 the surface, located at 45° with respect to the surface normal and to the incoming ion beam in the present experiments. From these elements it is obvious that most of the scattering, in a gas phase model, will scatter ions into the surface. For the present analysis we ignore the fate of these ions. Recoil of these ions from the surface may, in fact, account for some of the broadening observed experimentally.

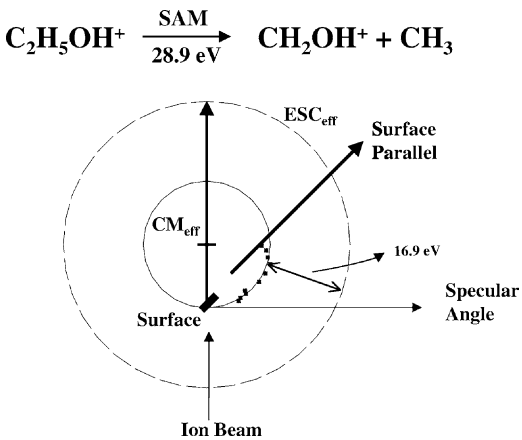

Fig. 14. A plot of the most probable velocities of fragment ions at 28.9 eV ion energy as a function of scattering angle. These points follow a circle whose center, marked as CM_{eff}, falls on the post-collision velocity vector. The cross marked CM_{SAM} corresponds to the CM of the collision between the ion and the SAM surface.

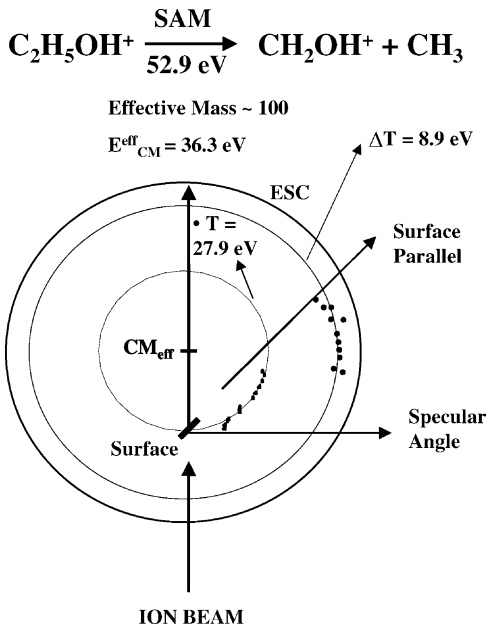

Fig. 15. A plot of the most probable velocities of fragment ions at 52.9 eV collision energy for the two highly inelastic SID processes. Velocities fall on circles with a common center located on the relative velocity vector and the center defines the effective mass of the collision partner.

We proceed to construct Figs. 14 and 15 by converting energy of ions into velocities using the $E = \frac{1}{2}mv^2$ relationship. The most probably velocities are plotted in Figs. 14 and 15, for 28.9 and 52.9 eV collision energy, respectively. In both figures the experimental data points are reasonably interpreted as falling on segments of circles with their origin on the relative velocity vector for the collision. Only one circle is shown in Fig. 14 because not enough points are available to define a second circle. Conventional analysis of the origin of these circles gives us the effective center-of-mass (CM) for the collision process. We can use this CM to estimate the mass of the collision partner as 117, which is close to the mass of the CF_3CF_2 group (119) at the end of the SAM molecular chain. Similar conclusions of the involvement of only a fraction of the surface molecular chain were made

by Nathanson and coworker [44] and Minton and coworkers [45] from collisions with liquid surfaces.

Fig. 15 shows two circles with a common origin at an effective mass of ∼100, somewhat less than the lower collision energy experiment. We do not attach any particular significance to the deduction that the effective masses correspond to C_2F_4 and C_2F_5 groups at the two collision energies. The essential point is that our pseudo-Newton diagrams support the concept that a terminal group rather than collective mass of the SAM surface is the effective collider for the highly inelastic scattering mechanisms.

Continuing this analysis, the location of these circles with respect to the elastic scattering circle (ESC) in gas phase collisions is a quantitative measure of energy transfer in the collision. The same analysis applied here gives energy deposition of ∼16.9 for 28.9 eV collisions and ∼8.9 and ∼27.9 eV for the two highly inelastic mechanisms found for 52.9 eV collisions. Since both colliders have internal modes, there is no way to partition this energy amongst them from this information alone. (We note that this is also true for gas phase experiments in which both the ion and neutral are polyatomic species.) Depositing such large amounts of energy in the ion would result in extensive fragmentation rather than generate the normal mass spectrum which is observed. Rather, the recoil of the terminal group compresses the chain and collective motions of the SAM efficiently dissipate ion impact energy into the surface, which is consistently found for the ions investigated so far. Accordingly, the success in our use of Newton diagrams to define the recoil of ions after surface impact is only one of the salient characteristics of CID dynamics. It does not account for energy transfer and cannot be considered a model for SID, at least in its present form.

Fig. 16 is a plot of points pseudo-Newton diagram data points for high energy fragment ions in which we plot the velocities as prompt and delayed dissociations corresponding to the assumptions of processing through the energy analyzer as *m*/*z* 31 and 46, respectively. Interestingly, if we assume that these fragment ions are due to collisions with the end group of the SAM surface as in Fig. 15, both sets of data points fall outside the ESC (for ethanol ions colliding with the C_2F_5 or C_2F_4 group), suggesting that these are highly exothermic processes. We have rejected earlier that such highly exothermic reactions are possible. The alternative assumption that the surface is rigid (e.g., in momentum exchange presents an infinite mass collider to the ion) is instructive. The ESC for this model falls just outside the data points corresponding to delayed dissociation while those for prompt dissociation fall well outside the circle. This supports and elaborates our earlier conclusion that this mechanism is delayed dissociation of a long-lived ethanol cation. For the delayed dissociation mechanism this analysis clearly suggests that ethanol ions interact with either the bulk surface or possibly with a number of SAM molecule chains simultaneously resulting in the behavior equivalent to bulk surface (of infinite mass).

3.4. Ar^+ scattering dynamics from the same SAM surface

The completely unanticipated dynamics observed for ethanol cations prompted us to explore briefly the scattering of Ar^+ at similar energies from the same SAM surface used in our SID study. Ar^+ ion has the advantages that no decomposition of the projectile ions is possible and Ar^+ scattering can be used as a probe of the dynamics of energy exchange with the surface. Except for inter-conversions involving the ground state doublet of the ion $^2P_{3/2}$, $^2P_{1/2}$, the lowest-lying electronically excited state of Ar^+ ($^2S_{1/2}$) is located 13.48 eV above Ar^+ ($^2P_{3/2}$). Consequently, it is unlikely that a significant fraction of Ar^+ are electronically excited.

The results from these preliminary experiments are summarized in Figs. 17–19. Fig. 17 summarizes the angular scattering of Ar^+ at a collision energy of 26.5 eV. This single mechanism is endothermic by ∼1.2 eV (not-shown) matching closely the scattering dynamics observed for inelastic scattering of ethanol cations (and the long-lived decomposition into CH_2OH^+) depicted in Figs. 6 and 7. This dynamics mechanism is the only one found for Ar^+ scattering at 26.5 eV collision energy.

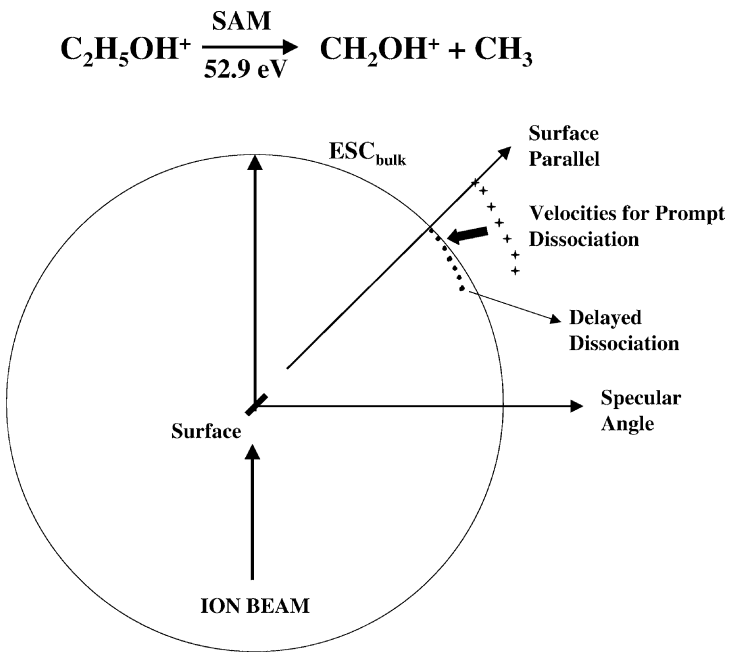

Fig. 16. Plot of the most probable velocities of the ions due to delayed dissociation. Corresponding most probable velocities for this process assuming prompt dissociation before the energy analyzer have also been drawn. The circle marked ESC_{bulk} corresponds to the elastic scattering circle for the collisions of ethanol ions with the bulk surface of infinite mass. The CM in this case corresponds to the collision center on the surface and the primary ion beam velocity is the radius of the elastic scattering circle.

Figs. 18 and 19 summarize the scattering dynamics of Ar^+ scattering from the SAM surface at 37.1 eV collision energy. Fig. 18 shows the angular scattering characteristics, while Fig. 19 shows the measured kinetic energies of Ar^+ after they are scattered from the surface. The scattering mechanism for which ions recoil nearly parallel to the surface is nearly elastic and clearly equivalent to the lower energy results

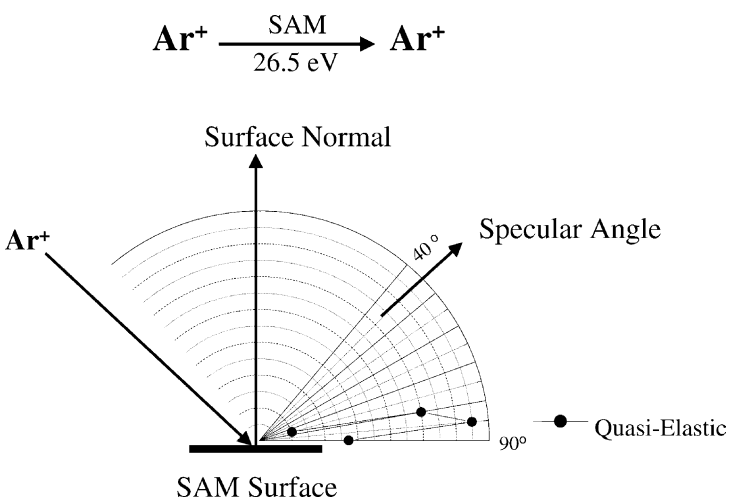

Fig. 17. A polar plot of the angular distribution of scattered Ar^+ ions from the SAM surface at 26.5 eV collision energy.

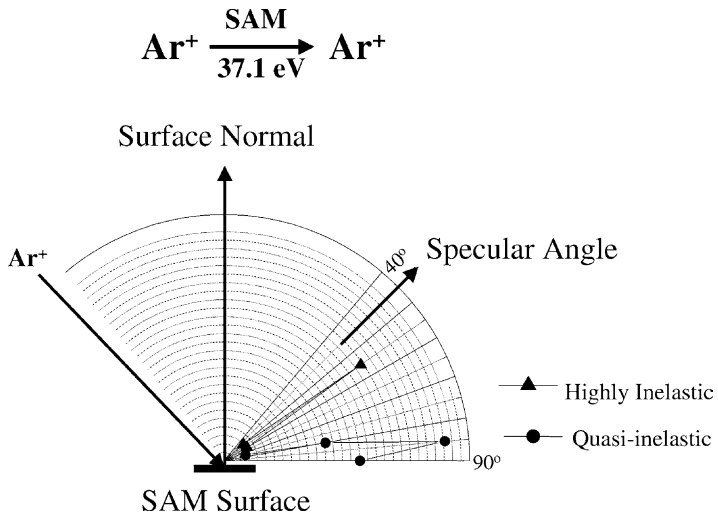

Fig. 18. A polar plot of the angular distribution of scattered Ar^+ ions from the SAM surface at 37.1 eV collision energy.

for Ar^+ and to the analogous dynamics found for ethanol cations. Surprisingly, a high translationally endothermic mechanism is also evident in Figs. 18 and 19. This scattering feature may involve electronic excitation of Ar^+, energy transfer to the SAM or a combination of both. These dynamics features are quite sharp, indicative of quite specific interactions in the collision process.

We consider the close agreement between Ar^+ scattering dynamics and ethanol cation scattering dynamics for product ions scattered parallel to the surface to be strong evidence that they follow the same kinds of surface interactions. That previous workers have not reported such dynamics feature is tentatively attributed to the different surfaces involved (fluorinated SAM, $C_{10}F_{21}C_2H_4SH$, reacted with a clean Au (1 1 1) surface vs. oil coated carbon and stainless steel surfaces and fluorinated SAM on gold coated glass substrate). Future studies will examine other surfaces, incident angle and tilt angles with respect to the ion beam.

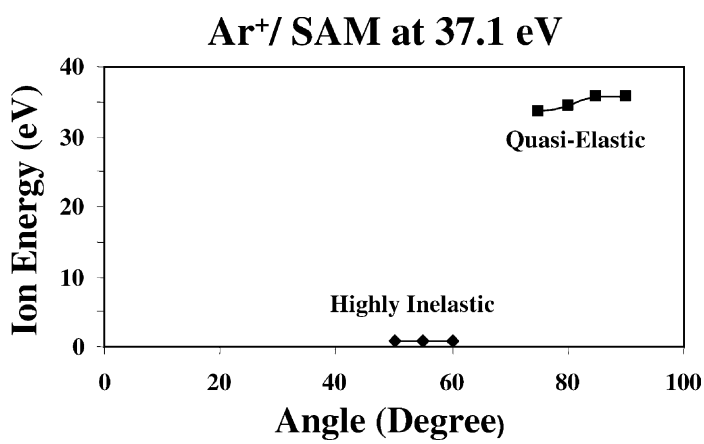

Fig. 19. A plot of the most probable kinetic energies of scattered Ar^+ ions of 37.1 eV collision energy, measured as a function of the scattering angle.

4. Conclusions

The experimental results for the SID of ethanol ions on a fluorinated SAM surface presented here demonstrate relatively complex reaction dynamics features that are dependent on the kinetic energy of impacting ions. Our results are, on the one hand, in good agreement with existing data for the same system and, on the other, reveal new and unexpected dynamics features. At lower energy, the majority of fragment ions are formed by highly inelastic collisions where most of the ions' kinetic energy is lost in collisions. However, only a small fraction of the kinetic energy is transferred into internal modes of dissociating ions. As ion energy is increased, an energetically distinct second inelastic channel opens up in addition to the nearly fully inelastic channel. Both SID processes have different angular distributions, suggesting that collisional energy transfer mechanisms are different for the two highly inelastic channels.

A new feature in SID dynamics is observed at both energies which is distinct in both angle and energy—sharply distributed close to the surface parallel—and only slightly endoergic. The dynamics of this feature are indistinguishable within experimental error to that observed for undissociated primary ions. Relative abundance of this mechanism increases in comparison with highly inelastic scattering as ion energy is increased. Since the scattering features and energy distributions for this process are essentially identical to that of the undissociated primary ethanol ions, we suggest that the same ion–surface collision dynamics result in formation of long-lived, excited primary ions which decompose after ions have passed through the energy analyzer.

Acknowledgements

This work was partially supported by Laboratory Directed Research and Development (LDRD) funds and partially supported by a Grant from the Department of Energy's Office of Basic Energy Sciences. We would like to thank Professor Vicki Wysocki (University of Arizona) for providing the surface material used for making SAM surface. We also thank members of the machine shop and instrument development lab for their continued support of our research facilities. William R. Wiley Environmental and Molecular Sciences Laboratory is the national user facility within the Pacific Northwest National Laboratory, operated by Battelle Memorial Institute for the U.S. Department of Energy under contract DE-AC06-76RLO-1830.

References

[1] J.W. Rabalais (Ed.), Low Energy Ion–Surface Interactions, Wiley, New York, 1994.
[2] H. Gnaser, Low Energy Ion Irradiation of Solid Surfaces, Springer, Berlin, 1999.
[3] A. Benninghoven, F.G. Rudenauer, H.W. Werner, Secondary Ion Mass Spectrometry: Basic Concepts, Instrumental Aspects, Applications and Trends, in: P.J. Elving, J.D. Winefordner (Eds.), Chemical Analysis, Wiley, New York, 1987.
[4] J.P. Briand, L. de Billy, P. Charles, S. Essabaa, P. Briand, J.P. Desclaux, R. Geller, S. Bliman, C. Ristori, Phys. Rev. Lett. 77 (1996) 1452.
[5] V. Grill, J. Shen, C. Evans, R.G. Cooks, Rev. Sci. Instrum. 72 (2001) 3149, and references cited therein.
[6] G. Tsaprailis, H. Nair, A. Somogyi, V.H. Wysocki, W. Zhong, J.H. Futrell, S.G. Summerfield, S.J. Gaskell, J. Am. Chem. Soc. 121 (1999) 5142.
[7] D.G. Schultz, H. Lim, S. Garbis, L. Hanley, J. Mass Spectrom. 34 (1999) 217.
[8] L. Schmidt, H.W. Fritsch, H. Jungclas, Rapid Commun. Mass Spectrom. 7 (1993) 507.
[9] W. Christen, U. Even, T. Raz, R.D. Levine, J. Chem. Phys. 108 (1998) 10262.
[10] J. Laskin, E. Denisov, J. Futrell, J. Am. Chem. Soc. 122 (2000) 9703.
[11] E.G. Stone, K.J. Gillig, B.T. Ruotolo, D.H. Russell, Int. J. Mass Spectrom. 212 (2001) 519.
[12] R.G. Cooks, T. Ast, M.A. Mabud, Int. J. Mass Spectrom. Ion Process. 100 (1990) 209.
[13] J.A. Burroughs, S.B. Wainhaus, L. Hanley, J. Phys. Chem. 98 (1994) 10913.
[14] H.L. de Clercq, A.D. Sen, A.K. Shukla, J.H. Futrell, Int. J. Mass Spectrom. 212 (2001) 491.
[15] R.G. Cooks, T. Ast, T. Pradeep, V. Wysocki, Acc. Chem. Res. 27 (1994) 316.
[16] A. Somogyi, T.E. Kane, J.M. Ding, V.H. Wysocki, J. Am. Chem. Soc. 115 (1993) 5275.
[17] B. Feng, J. Shen, V. Grill, C. Evans, R.G. Cooks, J. Am. Chem. Soc. 120 (1998) 8189.

[18] T. Pradeep, J.W. Shen, C. Evans, R.G. Cooks, Anal. Chem. 71 (1999) 3311.
[19] S.A. Miller, D.E. Riederer, R.G. Cooks, W.R. Cho, H.W. Lee, H. Kang, J. Phys. Chem. 98 (1994) 245.
[20] J. Laskin, E. Denisov, J. Futrell, J. Phys. Chem. B 105 (2001) 1895.
[21] D.G. Schultz, S.B. Wainhaus, L. Hanley, P. de Saint-Claire, W.L. Hase, J. Chem. Phys. 106 (1997) 10337.
[22] J. Kubista, Z. Dolejsek, Z. Herman, Eur. Mass Spectrom. 4 (1998) 311.
[23] A.K. Shukla, J.H. Futrell, A.D. Sen, J. Chem. Phys., in press.
[24] R. Worgotter, J. Kubista, J. Zabka, Z. Dolejsek, T.D. Mark, Z. Herman, Int. J. Mass Spectrom. Ion Process. 174 (1998) 53.
[25] J. Zabka, Z. Dolesjek, J. Roithova, V. Grill, T.D. Mark, Z. Herman, Int. J. Mass Spectrom. 213 (2002) 145.
[26] J. Zabka, Z. Dolejsek, Z. Herman, J. Phys. Chem. B, in press.
[27] (a) L. Hanley, H. Lim, D.G. Schultz, S.B. Wainhaus, P. de Saint Claire, W.L. Hase, Nucl. Instrum. Meth. Res. B 125 (1997) 218;
(b) D. Schultz, L. Hanley, J. Chem. Phys. 109 (1998) 10976.
[28] E. Hendell, U. Even, T. Raz, R.D. Levine, Phys. Rev. Lett. 75 (1995) 2670.
[29] I. Schek, J. Jortner, T. Raz, R.D. Levine, Chem. Phys. Lett. 257 (1996) 273.
[30] S.B.M. Bosio, W.L. Hase, Int. J. Mass Spectrom. Ion Process. 174 (1998) 1.
[31] O. Meroueh, W.L. Hase, J. Am. Chem. Soc. 124 (2001) 1524.
[32] O. Meroueh, Y. Wang, W.L. Hase, in press.
[33] A.K. Shukla, J.H. Futrell, Rev. Sci. Instrum., in press.
[34] NIST Standard Reference Data Base—1998, Chemistry Web Book.
[35] H. Akazawa, Y. Murata, J. Chem. Phys. 92 (1990) 5551.
[36] R.D. Levine, R.B. Bernstein, Molecular Reaction Dynamics and Chemical Reactivity, Oxford University Press, New York, 1987.
[37] J.H. Futrell (Ed.), Gaseous Ion Chemistry and Mass Spectrometry, Wiley, New York, 1986.
[38] R.A. Marcus, O.K. Rice, J. Phys. Colloid Chem. 55 (1951) 894.
[39] W.J. Bouma, R.H. Nobes, L. Radom, J. Am. Chem. Soc. 105 (1983) 1743.
[40] G. Bouchoux, N. Choret, Int. J. Mass Spectrom. 201 (2000) 161.
[41] R.G. Cooks, L. Hendricks, J.H. Beynon, Org. Mass Spectrom. 10 (1975) 625.
[42] A.J. Stace, A.K. Shukla, Int. J. Mass Spectrom. Ion Phys. 37 (1981) 35.
[43] A.K. Shukla, J.H. Futrell, Mass Spectrom. Rev. 12 (1993) 211.
[44] M.E. Saecker, G.M. Nathanson, J. Chem. Phys. 99 (1993) 7056.
[45] D.G. Garton, T.K. Minton, M. Alagia, N. Balucani, P. Casavecchia, G.G. Golpi, J. Chem. Phys. 112 (2000) 5975.